







# Demonstration of >1Tbit/s WDM OWC with wavelength-transparent beam tracking-and-steering capability

YANG HONG,<sup>1,\*</sup>  FENG FENG,<sup>2,3</sup> KYLE R. H. BOTTRILL,<sup>1</sup>   
NATSUPA TAENGOI,<sup>1</sup> RAVINDER SINGH,<sup>2,4</sup>  GRAHAME  
FAULKNER,<sup>2</sup> DOMINIC C. O'BRIEN,<sup>2</sup> AND PERIKLIS  
PETROPOULOS<sup>1</sup> 

<sup>1</sup>Optoelectronics Research Centre, University of Southampton, Southampton SO17 1BJ, United Kingdom

<sup>2</sup>Department of Engineering Science, University of Oxford, Oxford OX1 3PJ, United Kingdom

<sup>3</sup>Currently with School of Precision Instruments and Opto-Electronics Engineering, Tianjin University, Tianjin 300072, China

<sup>4</sup>Currently with Cambridge Research Laboratory, Toshiba Europe Limited, 208 Cambridge Science Park, Cambridge, CB4 0GZ, United Kingdom

\*y.hong@soton.ac.uk

**Abstract:** Beam tracking-and-steering is crucial for the operation of high-speed, narrow beam, optical wireless communication (OWC) systems. Using a system based on two sets of low-cost cameras for continuous beam tracking and a set of mirrors for steering, we demonstrate here a high-capacity (>1Tbit/s) ten-channel wavelength-division multiplexed (WDM) OWC system based on discrete multitone transmission. The results, which are achieved over a 3.5-m perpendicular distance and across a lateral coverage up to 1.8 m, constitute to the best of our knowledge, the highest aggregate OWC capacity at this coverage.

Published by The Optical Society under the terms of the [Creative Commons Attribution 4.0 License](https://creativecommons.org/licenses/by/4.0/). Further distribution of this work must maintain attribution to the author(s) and the published article's title, journal citation, and DOI.

## 1. Introduction

The ever growing use of multimedia devices supporting bandwidth-hungry applications has contributed to an exponential increase in the wireless data traffic in recent years [1–3]. However, conventional radio-frequency (RF) wireless communications is facing a looming spectrum crunch, hence both industry and academia are seeking supplementary techniques for the implementation of future high-speed wireless communications. Optical wireless communications (OWC), featuring the benefits of an unregulated wide bandwidth, immunity to electromagnetic interference and much higher achievable data rates than RF, is a promising candidate for both indoor and outdoor high-speed wireless access [1–3]. In broad terms, OWC systems can be divided into two categories: visible light communications (VLC) and infrared OWC. By directly modulating visible lighting sources, VLC can enable simultaneous illumination and data transmission, and has been investigated in different indoor/outdoor/underwater applications [4–7]. Despite numerous efforts to improve the performance of VLC systems, their transmission capability is relatively limited (to the order of gigabit/s), which is mainly due to the low bandwidth of the transceivers in the visible wavelength band [8–10]. In contrast, narrow-beam infrared OWC can offer a much higher achievable capacity by using fiber-optic devices in the fiber telecom-band. However, this is generally achieved at the expense of a significantly reduced coverage, since the field-of-view of such optical links is much narrower compared to that of VLC [11,12]. Furthermore, eye safety regulations restrict the maximum permissible emitted power at the transmitter (e.g. below 10 dBm for 1550 nm), according to the International Electrotechnical Commission Standard

[13]. For these reasons, sensitive beam tracking and steering systems are of great importance in infrared OWC systems.

In the literature, various active and passive techniques have been demonstrated to realize effective beam tracking, including micro-electromechanical system (MEMS) mirrors [14,15], spatial light modulators (SLMs) [16,17], optical phased arrays [18], Bragg gratings [19], arrayed waveguide grating routers (AWGRs) [20] and silicon photonic integrated circuits (PICs) [21]. While the point-to-point wavelength division multiplexed (WDM) OWC transmission can be realized by using the MEMS mirrors or SLMs for beam steering [15,17], issues like polarization sensitivity and implementation cost/complexity may compromise their uses in practical OWC systems. On the other hand, for the schemes that employ the PIC-integrated/grating-based phase arrays, Bragg gratings, or AWGRs, they do not easily lend themselves to point-to-point ultrahigh-speed WDM operation, since different wavelengths are steered to different locations (i.e., point-to-multipoint). To support point-to-point WDM transmission and thereby boost the capacity of OWC systems, wavelength-transparent beam steering is more desirable. In addition, beam tracking is also crucial for OWC systems to facilitate the support of user mobility. The user's localization can be identified by means of a wavelength-to-position mapping in AWGR-based OWC systems [20], provided that a pre-known lookup table is available. Furthermore, solutions like RF-assisted localization [22] or image sensor-based positioning [16,23–25] can also be used to track the user's location and then steer optical beams accordingly. By adopting a LED-tag system at the receiver (Rx), the camera-equipped transmitter (Tx) can localize the Rx within milliseconds at an accuracy of  $0.018^\circ$  [24]. Furthermore, upstream signalling can be enabled by modulating the LED tag at the Rx and detecting the signal with the help of the camera at the Tx, facilitating the simultaneous localization of a large number of OWC users [23,24]. In [25], a millimeter-scale positioning accuracy has been achieved using the LiDAR, and calibration-free OWC transmission at 17 Gb/s over a 3-m distance has been demonstrated. Using low-cost mirrors and cameras, we have previously demonstrated simultaneous beam tracking and steering, enabling high-speed WDM transmission based on 4-ary pulse amplitude modulation [26].

In this paper, we report the delivery of  $>1$ -Tb/s adaptively-loaded discrete multitone (DMT) transmission to a single optical wireless receiver over a distance of 3.5 m with a lateral coverage of up to 1.8 m. Thanks to the wavelength-transparent property of the mirror-based steering system, similar transmission performance was achieved for all ten WDM channels. Compared to the work presented in [26], more than 16% capacity enhancement and around 50% coverage improvement were simultaneously realized. This was achieved by using the DMT with adaptive bit and power loading, which exhibits the intrinsic capability of capacity maximization as well as superior bit error rate (BER) performance at low received optical power (ROP), when compared to our previously used 4-ary pulse amplitude modulation. Furthermore, the adoption of bit-rate adaptable DMT has allowed us to carry out a detailed investigation of the trade-off between transmission capacity and lateral coverage, thus providing a better understanding of the operation of the demonstrated beam tracking-and-steering system when used for high-speed transmission.

## 2. Experimental setup

### 2.1. Principle of the beam tracking-and-steering

The beam tracking-and-steering system has been described in detail elsewhere [26], hence is briefly outlined here for completeness.

A block diagram of the system is shown in Fig. 1(a). The optical signal at the Tx passes through an optical fiber collimator (Coll, *Thorlabs* TC06APC-1550), followed by a beam splitter, which is composed of a dichroic filter (DF) and a bandpass filter (BF). The diameter and full divergence of the resulting beam are around 1 mm and 0.101 degree, respectively. The direction of the emitted beam is controlled by a steering mirror (M1). Note that the mirror is gold-coated and exhibits  $>95\%$  reflectivity over a broad bandwidth (800 nm to 6  $\mu\text{m}$ ). Considering that the

narrow-beam property of the signal beam makes it challenging to realize a wide-range localization and tracking capability, in this work, a ring of 800-nm LEDs is arranged around the mirror and is used as a beacon (BCN1) for tracking. An identical setup is implemented at the Rx, except that the beacon (BCN2) comprises 890-nm LEDs. To realize bidirectional tracking, two wide field-of-view (FOV) cameras (CAM1 and CAM3) and two narrow FOV cameras (CAM2 and CAM4) are adopted. We note that using a separate tracking system at  $\sim 800$  to 900 nm enables the use of low-cost LEDs and tracking cameras, and the tracking functionality can be undertaken independently of any communications signal being present over a wide range. Different LED wavelengths at the Tx and Rx are used to avoid any interference in the tracking process and BFs are used on each tracking camera to ensure that only light from the beacons on the opposite terminal is detected. The wide FOV cameras find the rough positions of the opposite terminal by detecting the rings of LEDs, and provide an initial pointing estimate. The fine tracking cameras are placed in the optical path of the system, using the DFs to combine the communications and tracking paths. This centers their field of view on the steered axis of the optical system, allowing precise alignment of the terminals. The latency induced by the whole beam tracking-and-steering process is  $\sim 200$  ms, of which the coarse and fine tracking account for  $\sim 50$  ms and  $\sim 150$  ms, respectively. A detailed characterization of the tracking-and-steering performance, including the positioning error and the induced latency, has been presented in our prior work [26]. Figure 1(b) shows the fully-assembled unit (@Tx) within a metallic housing of approximately  $15 \times 14 \times 13$  cm. It is worth noting that the use of broadband optics ensured wavelength-transparent operation, thereby allowing WDM transmission for ultrahigh-speed OWC, as will be demonstrated in the rest of this paper.

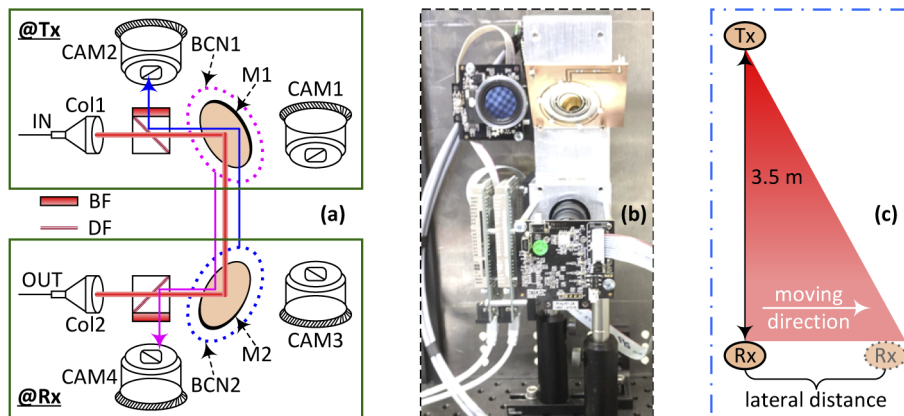


**Fig. 1.** (a) Diagram of the beam tracking-and-steering system, (b) the fully-assembled Tx, and (c) illustration of the relative placement of the Tx and Rx.

## 2.2. Transmission setup

For the transmission tests, the location of the Tx was fixed whilst laterally moving the Rx (see Fig. 1(c)). The vertical distance between Tx and Rx was 3.5 m. Due to the limited space available for the demonstration, the Rx was displaced laterally with respect to the Tx, but only on one direction (up to a distance of 0.9 m). However, considering that the properties of the steering mirrors and tracking cameras are symmetric [23], a full lateral coverage of 1.8 m can safely be assumed.

Figure 2 shows the block diagram of the WDM transmission setup and the corresponding digital signal processing (DSP) blocks of the direct-detection optical orthogonal frequency division multiplexing (DDO-OFDM) scheme that was used. Ten 100-GHz-spaced optical carriers

ranging from 1546.12 nm to 1553.33 nm were generated by ten continuous-wave lasers (*ID Photonics* CoBrite DX4) and then used for intensity modulation in a Mach-Zehnder modulator (MZM). The electrical signal generated from a 70-GSa/s arbitrary waveform generator (AWG) was first amplified before being used to drive the MZM. The output of the MZM was fed into a programmable filter (*Finisar* Waveshaper) to demultiplex the odd and even channels, which allowed for channel decorrelation by passing through different lengths of fibers. Subsequently, the decorrelated WDM channels were combined together and further amplified by an erbium-doped fiber amplifier (EDFA). The input power of the EDFA was around  $-6.6$  dBm and its output power was fixed at 18 dBm. A variable optical attenuator was used after the EDFA to ensure that the emitted optical power at the Tx was fixed at 9 dBm (below the eye safety limit). At the receiver, another EDFA was used to pre-amplify the received optical signal, and its output power was also fixed at 18 dBm. After the pre-amp EDFA, an optical bandpass filter (OBPF) was used to select each WDM channel in succession for performance evaluation. Another variable optical attenuator was used to adjust the ROP at the photodetector (PD), which was monitored through a 99:1 optical coupler. The detected signal at the PD was then recorded by an 80-GSa/s digital storage oscilloscope (DSO) for further offline DSP. It is worth noting that similar to some prior works [16,17,20,22–24], optical amplification has been adopted in this work. Although the use of two EDFAs introduces extra cost and power consumption, it facilitates the loss compensation of the OWC link and ensures high-speed transmission over ten WDM channels. As will be demonstrated later, with the help of the optical amplification, beyond Tbit/s OWC transmission over a wide coverage is achieved, which is also comparable to that demonstrated in amplified optical fiber communications. Nevertheless, we anticipate that such amplified OWC systems are more favourable in capacity-hungry applications that target at ultrahigh capacities.

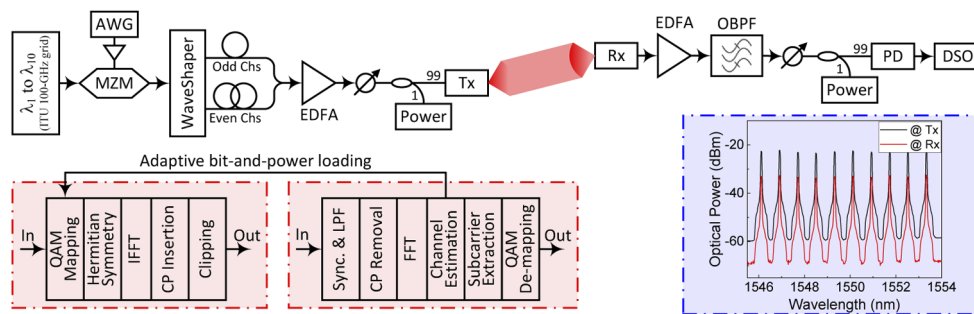


**Fig. 2.** Experimental setup of the WDM OWC transmission and the corresponding DSP blocks. Inset: comparison of the optical spectra of the ten WDM channels at the Tx and Rx.

As mentioned above, DDO-OFDM was considered in this work. At the transmitter in the offline DSP, Hermitian symmetry operation was applied to the quadrature amplitude modulation (QAM) mapped signal to ensure real-valued outputs after the inverse Fast Fourier transform (IFFT). The block size of the IFFT was 512, out of which 240 subcarriers were used to carry on data information, resulting in an overall signal bandwidth of 32.8125 GHz. After the IFFT, a cyclic prefix (CP) with a length of 1/8 of the DDO-OFDM symbol was inserted, and the resulting waveform was then clipped with a clipping ratio of 12 dB. At the receiver, the recorded data were first synchronized and low-pass filtered (LPF). After CP removal, FFT was performed to transform the time-domain signal into the frequency domain. Then, frequency-domain channel estimation (one-tap equalization) was conducted. The recovered QAM signals carried on the data subcarriers were subtracted accordingly and de-mapped to obtain the BER via error counting. For the adaptively-loaded DMT transmission, i.e., DDO-OFDM with adaptive loading [27], pilot

transmission based on DDO-OFDM was conducted first to estimate the channel state information, which was then used at the transmitter for adaptive bit and power loading.

### 3. Experimental results

We first evaluated the WDM OWC system using the 8QAM DDO-OFDM (98.4375 Gb/s per channel) when the Tx and Rx were vertically aligned, i.e., the lateral distance shown in Fig. 1(c) was 0 m. The link alignment was optimized to ensure minimum loss (10.5 dB) in the optical wireless link, and therefore optimal transmission performance. A comparison of the optical spectra of the ten WDM channels at the Tx and Rx is shown in the inset of Fig. 2. Figure 3 shows the corresponding transmission performance, including BERs and the average signal-to-noise ratio (SNR) versus ROP. Here, the average SNR refers to the mean value of the SNRs on all data subcarriers. As seen in the figure, similar performance was achieved for all ten WDM channels thanks to the wavelength-transparent property of the beam tracking-and-steering system. However, due to the limited bandwidth of the transceivers, the BERs were still higher than the 7% forward error correction (FEC) limit ( $3.8 \times 10^{-3}$ ) even at a ROP as high as  $-7$  dBm when the uniformly-loaded DDO-OFDM signals were used.

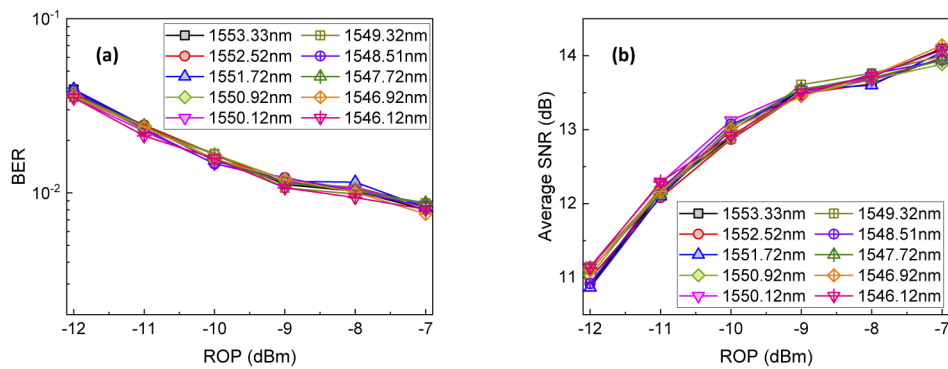
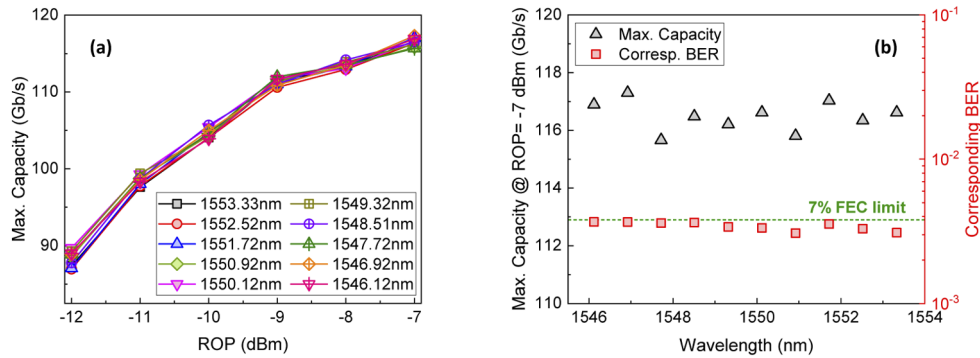


**Fig. 3.** Transmission performance versus ROP of the WDM OWC system using 8QAM DDO-OFDM at a lateral distance of 0 m: (a) BER and (b) average SNR.

To improve the BER performance as well as maximize the transmission capacity, we implemented adaptive bit-and-power loading, i.e., adaptively-loaded DMT, for each value of the ROP. Here, the objective of the adaptive loading was to maximize the capacity while keeping the corresponding BER lower than the 7% FEC limit [27,28]. Figure 4(a) shows the results of the adaptively-loaded DMT transmission for all channels under different ROP. It is clear that all channels shared comparable capacity performance. With a ROP higher than  $-11$  dBm, a rate beyond 100 Gb/s could be achieved for all channels. At the maximum ROP ( $-7$  dBm), the transmission capacity was around 116 Gb/s/channel whilst the corresponding BERs were all below the 7% FEC limit, as shown in Fig. 4(b).

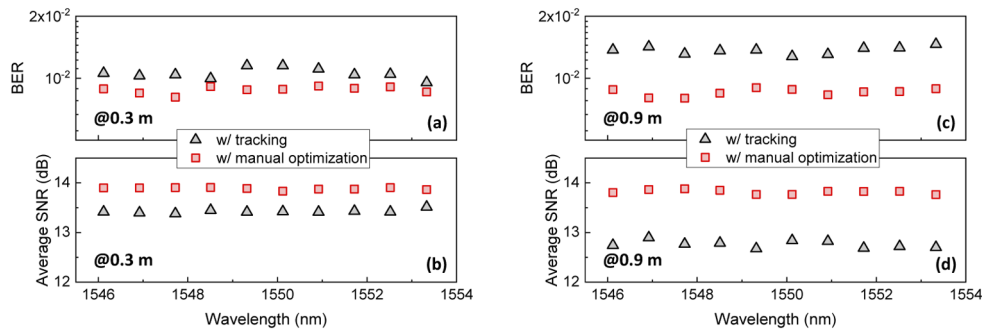
We next laterally moved the Rx (as indicated in Fig. 1(c)) to evaluate the beam tracking-and-steering capability of the system. Figure 5 shows the BER and average SNR results of the 8QAM DDO-OFDM WDM OWC transmission at lateral movements of 0.3 m and 0.9 m. The ROP was kept at  $-7$  dBm at both locations. Here, manual optimization, namely two-dimensional scanning of all possible angles of the steering mirrors to achieve the minimum link loss, was included as a benchmark for performance comparison. At a lateral distance of 0.3 m, the link loss when using either tracking only or manual optimization was 13.7 dB and 10.7 dB, respectively, whereas the corresponding values at the lateral distance of 0.9 m were 17 dB and 10.9 dB. Therefore, when increasing the lateral displacement, while the penalty introduced in the link loss was marginal by





**Fig. 4.** (a) Maximum capacity versus ROP of the WDM OWC system using adaptively-loaded DMT at a lateral distance of 0 m, and (b) Capacity of all ten WDM channels at a ROP of  $-7$  dBm and the corresponding BERs.

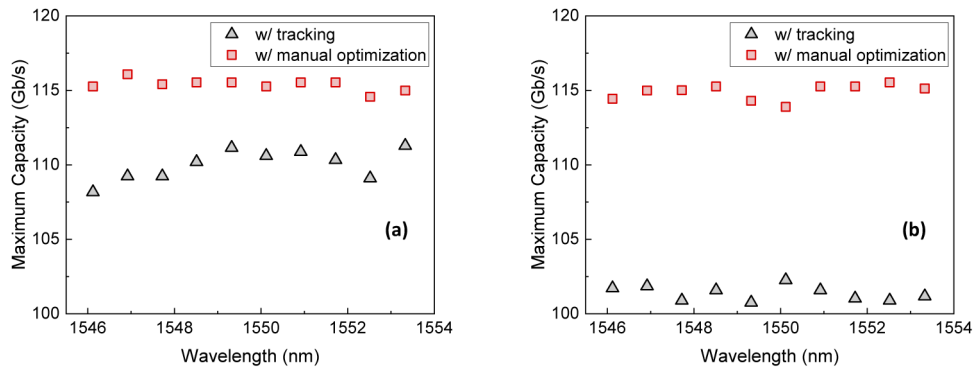
using manual optimization (0.2 dB), this value became significant when automatic tracking was employed (3.3 dB). This could result from the axial misalignment between the steering mirrors and cross-coupling between the mirror rotation axes [26].



**Fig. 5.** BER and average SNR performance of the ten channels with a lateral movement of (a-b) 0.3 m, and (c-d) 0.9 m. The modulation format and ROP were  $\sim 100$ -Gb/s 8QAM DDO-OFDM and  $-7$  dBm, respectively.

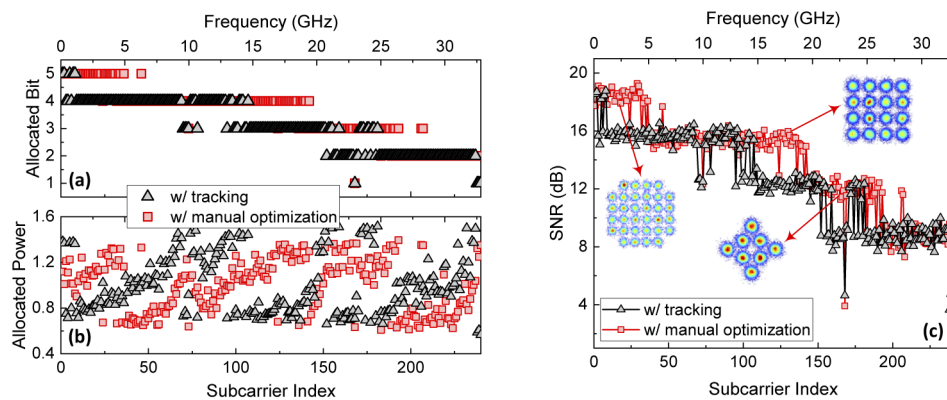
It is seen in Figs. 5(a-b) that for a lateral displacement of 0.3 m, the BER difference between using the automated tracking and manual optimization was relatively minor. Accordingly, only around 0.5-dB average SNR advantage was observed when manual optimization is performed. In contrast, when the lateral distance was further increased to 0.9 m (Fig. 5(c-d)), the transmission performance remained roughly the same regardless of the lateral movement when manual optimization was performed. However, its average SNR advantage over the automated tracking further increased to  $\sim 1$  dB and the corresponding BER difference also became more significant, due to the higher link loss. Nevertheless, the BERs of all channels were still below the 20% FEC limit ( $2 \times 10^{-2}$ ) under the 0.9-m lateral coverage when the automated tracking was adopted.

Figure 6 shows the results of the corresponding adaptively-loaded DMT transmission at the previous two lateral displacements at the same ROP of  $-7$  dBm. As expected, around 115-Gbit/s/channel capacity could be achieved in both cases when the manual optimization was used. In comparison, around 110-Gb/s/channel could be realized at a lateral distance of 0.3 m by using the tracking (Fig. 6(a)), whereas this value decreased to  $\sim 101$  Gb/s/channel when the lateral displacement was 0.9 m, as can be seen in Fig. 6(b).



**Fig. 6.** Maximum achievable capacity of the ten channels using the adaptively-loaded DMT with a lateral movement of (a) 0.3 m, and (b) 0.9 m. The ROP was  $-7$  dBm and the used BER threshold was the 7% FEC limit.

To illustrate the impact of the increased link loss on the transmission performance at large lateral distances, Fig. 7 further presents the results of bit- and power-loading as well as the corresponding SNR profiles of the 1553.33-nm channel for the case of 0.9-m lateral displacement. Due to the increased link loss in the case of tracking, and thus a lower optical SNR at the receiver, fewer bits were loaded to the data subcarriers, resulting in a lower capacity compared to that in the manual optimization case. In both cases, a saw-tooth behavior was observed in the power loading result, which helped maintain a similar BER and SNR performance for subcarriers loaded with the same order of QAM constellations, as shown in Figs. 7(b-c). For reference, the capacities in the tracking and manual optimization cases were around 101.72 Gb/s and 114.43 Gb/s whilst the corresponding BERs were  $3.43 \times 10^{-3}$  and  $3.60 \times 10^{-3}$ , respectively.



**Fig. 7.** Comparison of the adaptively-loaded DMT transmission results of the 1553.33-nm channel using tracking or manual optimization at a lateral distance of 0.9 m and a ROP of  $-7$  dBm: (a) allocated bit, (b) allocated subcarrier and (c) SNR profiles over data subcarriers.

A summary of the OWC system performance with increasing displacement is outlined in the graphs of Fig. 8. The graphs evaluate both the tracking and manual optimization schemes. Here, the total capacity was obtained using the adaptively-loaded DMT at the BER threshold of the 7% FEC limit. In the manual optimization case, the link loss increase was minor when compared to the minimum loss of 10.5 dB obtained at the position of no lateral displacement (as indicated in the dashed line shown in Fig. 8(a)). In comparison, in the tracking case, the link loss increased from 13.7 dB to 15 dB and 17 dB when the lateral distance was increased from 0.3 m

to 0.6 m and 0.9 m, respectively. Accordingly, around 1.15-Tb/s capacity was enabled across the 0.9-m coverage (single-side) in the manual optimization case, which represents a minor capacity reduction with regard to the maximum capacity of 1.16-Tb/s at the no-lateral-displacement position. In contrast, this total capacity reduced from  $\sim 1.10$  Tb/s to  $\sim 1.07$  Tb/s when the lateral distance was increased from 0.3 m to 0.6 m. Nevertheless,  $>1$ -Tb/s capacity was still achievable after a lateral movement up to 0.9 m ( $\sim 1.01$  Tb/s). As mentioned above, considering the inherent symmetrical property of the tracking and steering system, beyond 1-Tb/s transmission was enabled for a full lateral coverage of 1.8 m (double-side) whilst keeping the corresponding BER below the 7% FEC limit.

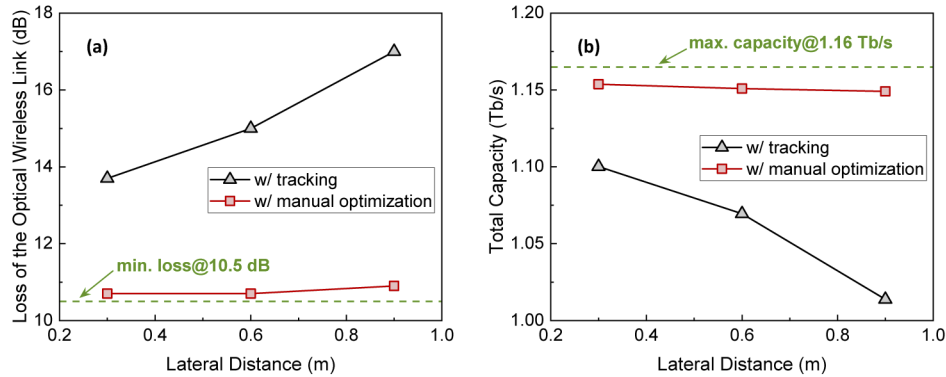


**Fig. 8.** Comparison of (a) link loss and (b) achievable capacity versus lateral distance using tracking or manual optimization at a ROP of  $-7$  dBm.

#### 4. Conclusions

In this paper, we demonstrated an ultrahigh-speed OWC transmission with simultaneous beam tracking-and-steering capability. The beam tracking-and-steering system was built with low-cost cameras and mirrors, and offered a low connection latency of 200 ms and wavelength-transparent operation. Based on a ten-channel WDM IM/DD system, we achieved  $>1$ -Tb/s capacity at a perpendicular distance of 3.5 m with a lateral coverage up to 1.8 m. It was also further demonstrated that, by using a more complex manual optimization, around 1.15-Tb/s capacity was achieved across the same coverage. The demonstrated beam trackable and steerable OWC system provides a viable route to achieving ultrahigh-speed connections in future indoor access networks.

**Funding.** Engineering and Physical Sciences Research Council (EP/P003990/1); Horizon 2020 Framework Programme (761329).

**Disclosures.** The authors declare no conflicts of interest.

**Data availability.** Data underlying the results presented in this paper are available in Ref. [29].

#### References

1. T. Koonen, "Indoor optical wireless systems: technology, trends, and applications," *J. Lightwave Technol.* **36**(8), 1459–1467 (2018).
2. A. Nirmalathas, C. Ranaweera, K. Wang, Y. Yang, I. Akhter, C. Lim, E. Wong, and E. Skafidas, "Photonics for gigabit wireless networks," in *Proc. of OFC, OSA Technical Digest Series* (Optical Society of America, 2015), paper W4G.3.
3. H. Haas, L. Yin, Y. Wang, and C. Chen, "What is LiFi?" *J. Lightwave Technol.* **34**(6), 1533–1544 (2016).
4. Y. F. Huang, C. T. Tsai, H. Y. Kao, Y. C. Chi, H. Y. Wang, T. T. Shih, and G. R. Lin, "17.6-Gbps universal filtered multi-carrier encoding of GaN blue LD for visible light communication," in *Proc. of CLEO (IEEE, 2017)*, paper STh1C.5.
5. X. You, J. Chen, and C. Yu, "Performance of location-based equalization for OFDM indoor visible light communications," *IEEE Trans. Cogn. Commun. Netw.* **5**(4), 1229–1243 (2019).



6. R. Deng, J. He, Z. Zhou, J. Shi, M. Hou, and L. Chen, "Experimental demonstration of software-configurable asynchronous real-time OFDM signal transmission in a hybrid fiber-VLLC system," *IEEE Photonics J.* **9**(1), 7801008 (2017).
7. M. Kong, W. Lv, T. Ali, R. Sarwar, C. Yu, Y. Qiu, F. Qu, Z. Xu, J. Han, and J. Xu, "10-m 9.51-Gb/s RGB laser diodes-based WDM underwater wireless optical communication," *Opt. Express* **25**(17), 20829–20834 (2017).
8. Y. Hong and L. K. Chen, "Toward user mobility for OFDM-based visible light communications," *Opt. Lett.* **41**(16), 3763–3766 (2016).
9. X. Huang, Z. Wang, J. Shi, and N. Chi, "1.6 Gbit/s phosphorescent white LED based VLC transmission using a cascaded pre-equalization circuit and a differential outputs PIN receiver," *Opt. Express* **23**(17), 22034–22042 (2015).
10. Y. Hong, L. K. Chen, and J. Zhao, "Performance-enhanced gigabit/s MIMO-OFDM visible light communications using CSI-free/dependent precoding techniques," *Opt. Express* **27**(9), 12806–12816 (2019).
11. T. Song, A. Nirmalathas, C. Lim, E. Wong, K. L. Lee, K. Alameh, and K. Wang, "Optical wireless communications adopting delay-tolerant repetition-coding with orthogonal-filters and on-demand equalization," *J. Lightwave Technol.* **38**(16), 4250–4259 (2020).
12. Y. Shao, Y. Hong, Z. Hu, and L. K. Chen, "Capacity maximization of OWC systems via joint precoding and probabilistic shaping," *IEEE Photonics Technol. Lett.* **31**(13), 1013–1016 (2019).
13. International Electrotechnical Commission Standard: Safety of optical fibre communication systems (IEC, 2018). <https://webstore.iec.ch/publication/62241>.
14. K. Wang, A. Nirmalathas, C. Lim, K. Alameh, and E. Skafidas, "Full-duplex gigabit indoor optical wireless communication system with CAP modulation," *IEEE Photonics Technol. Lett.* **28**(7), 790–793 (2016).
15. K. Kagawa and J. Tanida, "Demonstration of wide-angle beam steering optics in wavelength-division-multiplexing indoor optical wireless LAN with dedicated CMOS imager," in *Proc. of BIONETICS*, (ACM, 2008), pp. 1–6.
16. A. Gomez, K. Shi, C. Quintana, G. Faulkner, B. C. Thomsen, and D. O'Brien, "A 50 Gb/s transparent indoor optical wireless communications link with an integrated localization and tracking system," *J. Lightwave Technol.* **34**(10), 2510–2517 (2016).
17. A. Gomez, K. Shi, C. Quintana, R. Maher, G. Faulkner, P. Bayvel, B. C. Thomsen, and D. O'Brien, "Design and demonstration of a 400 Gb/s indoor optical wireless communications link," *J. Lightwave Technol.* **34**(22), 5332–5339 (2016).
18. J. K. Doyle, M. J. R. Heck, J. T. Bovington, J. D. Peters, L. A. Coldren, and J. E. Bowers, "Two-dimensional free-space beam steering with an optical phased array on silicon-on-insulator," *Opt. Express* **19**(22), 21595–21604 (2011).
19. Z. Yaqoob, M. A. Arain, and N. A. Riza, "High-speed two-dimensional laser scanner based on Bragg gratings stored in photothermorefractive glass," *Appl. Opt.* **42**(26), 5251–5262 (2003).
20. T. Koonen, F. Gomez-Agis, F. Huijskens, K. A. Mekonnen, Z. Cao, and E. Tangdionga, "High-capacity optical wireless communication using two-dimensional IR beam steering," *J. Lightwave Technol.* **36**(19), 4486–4493 (2018).
21. K. Wang, A. Nirmalathas, C. Lim, E. Wong, K. Alameh, H. Li, and E. Skafidas, "High-speed indoor optical wireless communication system employing a silicon integrated photonic circuit," *Opt. Lett.* **43**(13), 3132–3135 (2018).
22. A. M. Khalid, P. Baltus, A. R. Dommele, K. A. Mekonnen, Z. Cao, C. W. Oh, M. K. Matters, and A. M. J. Koonen, "Bi-directional 35-Gbit/s 2D beam steered optical wireless downlink and 5-Gbit/s localized 60-GHz communication uplink for hybrid indoor wireless systems," in *Proc. of OFC, OSA Technical Digest Series* (Optical Society of America, 2017), paper Th1E.6.
23. N. Q. Pham, K. A. Mekonnen, E. Tangdionga, A. Mefleh, and A. M. J. Koonen, "Multi-user localization and upstream signaling for indoor OWC system using a camera technology," in *Proc. of OFC, OSA Technical Digest Series* (Optical Society of America, 2020), paper M1J.7.
24. N. Q. Pham, K. Mekonnen, E. Tangdionga, A. Mefleh, and T. Koonen, "User localization and upstream signaling for beam-steered infrared light communication system," *IEEE Photonics Technol. Lett.* **33**(11), 545–548 (2021).
25. Z. Li, Z. Zang, M. Li, and H. Y. Fu, "LiDAR integrated high-capacity indoor OWC system with user localization capability," in *Proc. of OFC, OSA Technical Digest Series* (Optical Society of America, 2021), paper Tu5E.2.
26. R. Singh, F. Feng, Y. Hong, G. Faulkner, R. Deshmukh, G. Vercasson, O. Bouchet, P. Petropoulos, and D. O'Brien, "Design and characterisation of Terabit/s capable compact localisation and beam-steering terminals for fiber-wireless-fiber links," *J. Lightwave Technol.* **38**(24), 6817–6826 (2020).
27. Y. Hong, F. Feng, K.R.H. Bottrill, N. Taengnoi, R. Singh, G. Faulkner, D. C. O'Brien, and P. Petropoulos, "Beyond Terabit/s WDM optical wireless transmission using wavelength-transparent beam tracking and steering," in *Proc. of OFC, OSA Technical Digest Series* (Optical Society of America, 2020), paper W1G.4.
28. P. S. Chow, J. M. Cioffi, and J. A. C. Bingham, "A Practical Discrete Multitone Transceiver Loading Algorithm for Data Transmission over Spectrally Shaped Channels," *IEEE Trans. on Commun.* **43**(2/3/4), 773–775 (1995).
29. Y. Hong, F. Feng, K. R. H. Bottrill, N. Taengnoi, R. Singh, G. Faulkner, D. C. O'Brien, and P. Petropoulos, "Dataset for: Demonstration of >1Tbit/s WDM OWC with wavelength-transparent beam tracking-and-steering capability," (University of Southampton, 2021). <https://doi.org/10.5258/SOTON/D1921>.